Visual experience sculpts whole-cortex spontaneous infraslow activity patterns through an Arc-dependent mechanism

Andrew W. Kraft[a], Anish Mitra[b], Adam Q. Bauer[b], Abraham Z. Snyder[a,b], Marcus E. Raichle[a,b], Joseph P. Culver[b,c,d], and Jin-Moo Lee[a,b,c,1]

[a]Department of Neurology, Washington University in St. Louis, St. Louis, MO 63130; [b]Department of Radiology, Washington University in St. Louis, St. Louis, MO 63130; [c]Department of Biomedical Engineering, Washington University in St. Louis, St. Louis, MO 63130; and [d]Department of Physics, Washington University in St. Louis, St. Louis, MO 63130

Decades of work in experimental animals has established the importance of visual experience during critical periods for the development of normal sensory-evoked responses in the visual cortex. However, much less is known concerning the impact of early visual experience on the systems-level organization of spontaneous activity. Human resting-state fMRI has revealed that infraslow fluctuations in spontaneous activity are organized into stereotyped spatiotemporal patterns across the entire brain. Furthermore, the organization of spontaneous infraslow activity (ISA) is plastic in that it can be modulated by learning and experience, suggesting heightened sensitivity to change during critical periods. Here we used wide-field optical intrinsic signal imaging in mice to examine whole-cortex spontaneous ISA patterns. Using monocular or binocular visual deprivation, we examined the effects of critical period visual experience on the development of ISA correlation and latency patterns within and across cortical resting-state networks. Visual modification with monocular lid suturing reduced correlation between left and right cortices (homotopic correlation) within the visual network, but had little effect on internetwork correlation. In contrast, visual deprivation with binocular lid suturing resulted in increased visual homotopic correlation and increased anti-correlation between the visual network and several extravisual networks, suggesting cross-modal plasticity. These network-level changes were markedly attenuated in mice with genetic deletion of Arc, a gene known to be critical for activity-dependent synaptic plasticity. Taken together, our results suggest that critical period visual experience induces global changes in spontaneous ISA relationships, both within the visual network and across networks, through an Arc-dependent mechanism.

infraslow activity | functional connectivity | visual critical period | activity-regulated cytoskeleton-associated protein

During the visual critical period, neurons within the visual cortex exhibit robust plasticity in response to visual stimuli. Binocular visual input during this period is required for the proper development of normal visual cortex function (1–5). This experience-dependent activity drives a cascade of events leading to the development of mature response properties, such as ocular dominance, orientation selectivity, spatial acuity, and others, to produce normal adult vision (1, 2, 4–8). As first demonstrated by Hubel and Wiesel, binocular and monocular deprivation alter the response of visual cortex neurons to visual stimuli in distinct ways: Binocular deprivation prevents maturation of normal visual responses, causing immature visual responses to be retained, whereas monocular deprivation induces robust ocular dominance plasticity (ODP), actively depressing deprived eye responses (1, 2, 4–7). These effects have been demonstrated at multiple spatial scales spanning single neuron electrophysiology (4, 6) to entire visual hemicortex responses (9–11) in several species, including primates, cats, ferrets, rats, and mice (1, 4–10, 12). Moreover, the visual deprivation paradigm has illuminated the molecular mechanisms that drive experience-dependent visual plasticity. However,

the outcome measure in almost all prior studies has been limited to visual stimulus-evoked responses within the visual cortex.

Notwithstanding the scientific gains obtained by studying sensory-evoked responses, it is increasingly recognized that spontaneous (intrinsic) neural activity represents a complementary and productive line of investigation (13–15). Spontaneous activity accounts for the majority of brain activity and is thought to play a critical role in brain function (16, 17). The brain exhibits spontaneous activity at multiple temporal scales. Spontaneous infraslow activity (ISA; 0.01–0.1 Hz), initially regarded as "noise" (18), is now known to reflect properties of whole-brain network organization (19–23). Organized spontaneous activity has been observed using multiple imaging modalities, including resting-state fMRI (RS-fMRI) and optical imaging, in multiple species, including humans, nonhuman primates, and rodents (16, 17, 19, 24–26). More specifically, network organization is observed by patterns of spontaneous ISA correlation (termed functional connectivity; FC) and spontaneous ISA propagation speed between separate brain regions.

Human RS-fMRI studies have shown that the general organization of spontaneous ISA correlation and propagation is quite stable within and across individuals (22, 27). However, sensory experience and learning can modulate spontaneous ISA patterns at the systems scale. Specifically, motor learning (21, 28), extended Law School Admission Test (LSAT) preparation (29), and early

Significance

Visual critical periods are essential for shaping the normal mature responsiveness of visual cortex neurons; however, it is unclear whether early visual experience influences functional network organization. Here we demonstrate that monocular and binocular visual deprivation (MD and BD) have distinct effects on cortical functional connectivity (FC). MD induces FC changes restricted to the visual system, while BD results in widespread FC changes between disparate brain regions. These results suggest that early exposure to altered vision (MD) induces intranetwork change, but absent vision (BD) drives internetwork change, reminiscent of cross-modal plasticity. Moreover, this early experience-driven FC change was attenuated by deletion of Arc, a gene critical for synaptic plasticity, suggesting that network relationships are modulated by changes in synaptic strengths.

Fig. 1. Visual deprivation paradigm. (*A*) Experimental timeline for eyelid suturing and imaging. (*B*) Genotypes and deprivation groups used in this study: WT, Arc$^{-/-}$, BD, and MD. (*C*) Cartoon of mouse visual anatomy high-lighting monocular (solid) and binocular areas (striped).

age blindness (30–32) have all been demonstrated to alter ISA correlation in humans. Moreover, the magnitude of these effects correlated with behavioral measures (28). However, little is known regarding the mechanisms underlying systems-level modulation of spontaneous ISA organization. A leading hypothesis is that experience-dependent ISA modulation reflects brain plasticity. It is widely believed that plasticity at the systems level may be driven by mechanisms at the molecular level, especially those involving the modulation of synaptic strengths. However, there has been to date no evidence linking synaptic plasticity mechanisms, which operate on the spatial scale of microns (33), with the systems-scale ISA modulations occurring on the scale of centimeters (21, 28–31).

Of particular interest is that these spontaneous activity changes involve relationships between distinct functional systems, sug-gesting a paradigm of experience-dependent cross-modal plasticity that operates at the level of spontaneous activity. Although there already exists substantial evidence that visual loss in humans has extravisual, or cross-modal, effects on spontaneous ISA organi-zation throughout the cerebral cortex (30, 31), the role of critical period visual input on whole-cortex spontaneous ISA spatiotem-poral organization has not been examined.

To understand how critical period visual experience modulates whole-cortex ISA, we utilized functional optical intrinsic signal (fOIS) imaging in mice after binocular deprivation (BD) or mon-ocular deprivation (MD) during the visual critical period. We sub-sequently tested the role of synaptic plasticity in systems-level ISA reorganization by applying this paradigm to mice with genetic de-letion of activity-dependent cytoskeleton-associated protein (Arc). Several studies performed on a fine-spatial scale have established that Arc is essential for experience-dependent synaptic plasticity, largely through action on glutamate receptors (34–37). However, a role for Arc in systems-level ISA plasticity has not been studied.

Results

Visual Deprivation and ISA Imaging Paradigm. We manipulated vi-sual experience via lid suturing in mice at the beginning of the visual critical period (immediately after weaning at P21). Litter-mates were subjected to either (*i*) binocular lid suturing (i.e., BD), (*ii*) monocular right lid suturing (i.e., MD), or (*iii*) no lid suturing (normal vision; NV). A schematic of the experimental design is depicted in Fig. 1. After lid suturing, mice were returned to cages with littermates. Two weeks later (P35), fOIS imaging was per-formed to measure ISA. All mice tolerated the suturing and im-aging procedures well without mortality or morbidity.

ISA Spatiotemporal Organization Analysis. As shown in Fig. 2, we examined two features of the spatiotemporal organization in spontaneous ISA: zero-lag temporal correlations (FC) and temporal delays (propagation latency). Zero-lag correlations spatially partition the cortex into segregated functional networks known as resting-state networks (RSNs) that provide a spatial view of the system-level cortical organization (22, 38). More recent work has shown that ISA also exhibits temporal rela-tionships manifesting as reproducible propagation latency pat-terns, which can be computed by analyzing temporal delays (20, 21). Fig. 2 illustrates how correlation and propagation latency metrics were derived from a sample 20-s epoch of spontaneous ISA data from a single mouse (Fig. 2*A*). To define ROIs for analysis, we performed principal component analysis (PCA) parcellation using functional connectivity data from all mice (including both genotypes and all experimental conditions) used in this study (Fig. 2*B*). This method has been used to define
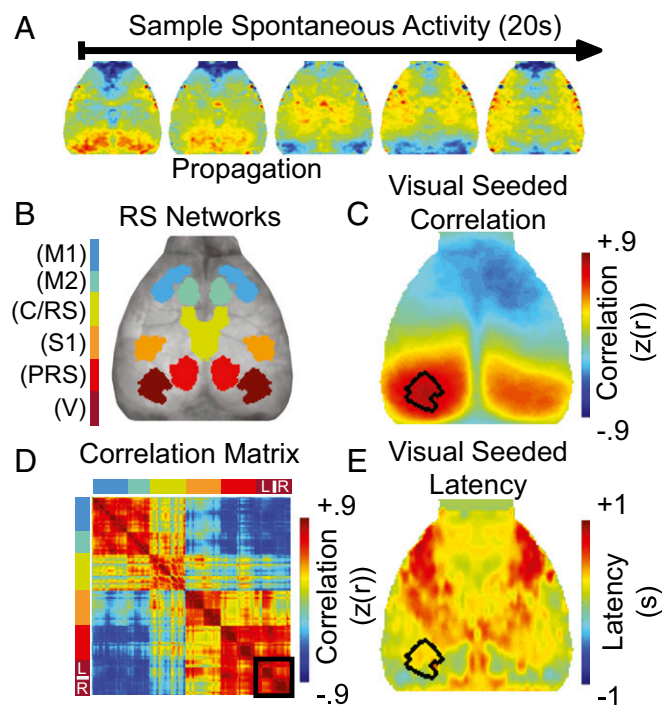
Fig. 2. Analysis of ISA correlation and propagation patterns for 20 s of data from a single mouse. (*A*) Frames from a sample movie showing 20 s of spon-taneous ISA from a single mouse. In this example, activity propagates from the posterior to anterior regions. Note that although ISA fluctuates over 10 to 100s of seconds, propagation occurs more quickly (~2 s in this example). Correlation between separate regions over the entire 20 s is present and especially ap-parent between homotopic interhemispheric regions throughout the cortex. (*B*) RSN parcellation of mouse cortex on the basis of PCA of group-level cor-relation structure (*Methods*). (*C*) Left visual-seeded correlation map from the sample data shows high correlation between left and right visual areas along with anticorrelation between the left visual and anterior regions. (*D*) Corre-lation matrix showing the correlation value for every pixel pair in the cortex from the sample ISA in *A*, organized by RSNs produced from *B* (color-coded on right). Within each RSN, left hemisphere pixels are sorted above right hemi-sphere pixels. This sorting offers a more detailed picture of correlation to-pography than what is viewable with a single correlation map. The visual RSN is outlined in the black box (*D*). The off diagonals (the top right or bottom left corner of the matrix) showed very high correlation between the left and right visual areas, in accordance with what is seen in the ISA sample in *A* and visual-seeded map in *C*. (*E*) Left visual-seeded activity propagation latency map of sample ISA in *A* shows early activity in the posterior region and later activity in the more anterior regions, consistent with what is seen in the sample ISA. C/RS, cingulate/retrosplenial; M1, primary motor; M2, secondary motor; PRS, pos-terior retrosplenial; S1, primary sensory; V, visual.

RSNs in human fMRI data previously (39). PCA parcellation resulted in RSNs that were labeled based on overlap with Paxinos atlas coordinates (24). ISA correlation in the present report is described both in terms of left visual-seeded correlation maps (corresponding to right-eye visual manipulation; Fig. 2C) as well as RSN-sorted correlation matrices (Fig. 2D). Propagation was examined with left visual-seeded latency maps displaying the earliness or lateness of each pixel relative to the left visual area (Fig. 2E; described further in *Methods*). Together, these approaches were used to quantify the effects that critical period visual experience had on the correlation and propagation latency patterns in spontaneous cortical ISA.

Visual Deprivation Alters ISA Correlation (FC). To determine if visual manipulation during the critical period alters ISA correlation, we examined visual-seeded correlation maps in WT mice with normal visual experience (WT-NV), binocular deprivation (WT-BD), and monocular deprivation (WT-MD) at P35 (after 2 wk of visual deprivation; Fig. 3 A–C). We chose to examine correlations for each pixel relative to the average signal of all left visual RSN pixels, because MD was applied to the right eye. In all groups, left visual-seeded correlation maps demonstrated high correlation

with the right visual cortex and anticorrelation to the more anterior regions, especially on the contralateral hemisphere. Statistical significance of correlation differences between groups was assessed with a spatial clusterwise basis using threshold-extent criteria computed by extensive permutation resampling (Fig. 3 D and E; see *Methods* for further detail). Comparing WT-BD to WT-NV demonstrated that BD resulted in increased homotopic correlation within the visual RSN (increased correlation between the interhemispheric visual areas) and increased anticorrelation between the visual and anterior areas (Fig. 3D). More specifically, these anterior areas included the primary motor (M1) and secondary motor (M2) areas as well as the anterior edge of the cingulate/retrosplenial area (Fig. 3D). Many pixels with significantly altered correlation to the left visual area fell just outside of the PCA-derived RSNs; according to Paxinos atlas coordinates, the area of increased anticorrelation (blue) was in anterior cingulate cortex (Fig. S1). MD, however, resulted in dramatically decreased homotopic visual correlation (within the visual network), but very little change in extravisual network correlation (Fig. 3E and Fig. S1), effects in stark contrast to those found with BD.

Interestingly, with both BD and MD there were no changes in correlation between the visual cortices and adjacent brain regions: correlation changes were restricted to longer distance connections. Histograms of visual homotopic correlation values demonstrate that BD and MD were shifted in opposite directions relative to NV: BD enhanced cross-hemispheric visual correlation, whereas MD disrupted it (Fig. 3F). Comparing BD to NV using anticorrelation histograms between visual and nonvisual pixels showed a dramatic increase in anticorrelation between visual and extravisual areas (Fig. 3G). MD, however, induced only a small effect on anticorrelation between visual and extravisual areas (Fig. 3G).

To examine ISA correlation changes related to visual manipulation at a more global level, we next created RSN-sorted correlation matrices, similar to that shown in Fig. 2D (but using the entire group-averaged data set rather than a sample 20-s epoch). These matrices demonstrated correlation and anti-correlation between networks in all three WT groups (Fig. 4 A–C). By definition, intranetwork correlation (diagonal blocks) was high, with prominent homotopic correlation in most RSNs, as has been shown previously in multiple mammalian species using optical and magnetic resonance imaging modalities (19, 24, 40, 41). Anticorrelation was apparent along the anterior–posterior axis both within and across hemispheres. The overall qualitative topography of correlation patterns was preserved between groups, but there were clear differences in correlation values.

To examine differences quantitatively at the whole-cortex level, we examined the correlation difference (Δcorrelation) matrices calculated by subtracting the WT-BD or WT-MD correlation matrices from the WT-NV correlation matrix (Fig. 4 D and G). These Δcorrelation matrices highlight the contrasting effects induced by BD and MD. The black outlines in Fig. 4 D and G, which highlight the visual RSN, demonstrate the increased visual intranetwork homotopic correlation seen in WT-BD vs. WT-NV (red off-diagonal blocks) and the decreased visual intranetwork homotopic correlation in WT-MD vs. WT-NT (blue off-diagonal blocks). Outside of the visual RSN, the anterior–posterior internetwork correlation differences had higher magnitude and opposite direction in the WT-BD minus WT-NV Δcorrelation matrix compared with the WT-MD minus WT-NV Δcorrelation matrix. Thus, in alignment with our visual-seeded analysis, the effects of visual deprivation were most pronounced in connections involving the visual areas, with the sign of change for each connection largely opposite in the BD vs. MD groups.

To determine statistical significance of whole-cortex correlation changes in WT with NV, BD, or MD, we computed the Δcorrelation matrix (WT-BD minus WT-NV and WT-MD minus WT-NV) over all pixels in the mouse cortex (instead of the subset of pixels included in the parcellation), and subjected this
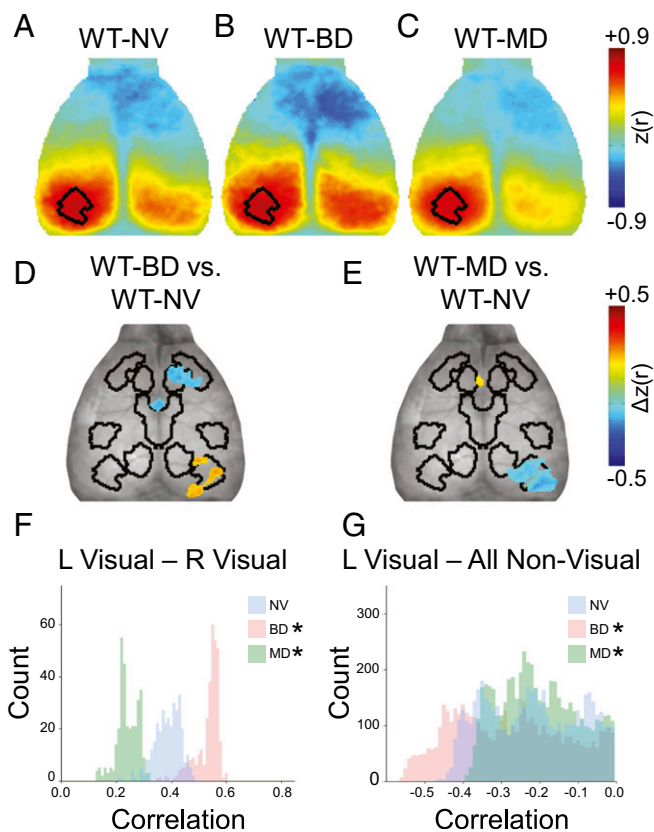
Fig. 3. Critical period visual deprivation alters visual-seeded ISA correlation patterns. (A–C) Group-level correlation maps seeded in the left visual RSN in (A) WT-NV, (B) WT-BD, and (C) WT-MD mice. (D) Statistically significant correlation differences between WT-NV and WT-BD mice based on spatial clusterwise threshold-extent criteria (*Methods*). Cool-colored pixels show decreased correlation in WT-BD compared with WT-NV, and warm-colored pixels show increased correlation in WT-BD compared with WT-NV mice. (E) Statistically significant correlation differences between WT-NV and WT-MD mice. (F) Correlation histograms between all right visual RSN pixels and the left visual RSN. (G) Correlation histograms between all nonvisual pixels (both within and outside of RSNs in Fig. 2B) and the left visual RSN. BD enhances interhemispheric intranetwork correlation and increases internetwork anticorrelation, and MD reduces intranetwork correlation with little effect on internetwork correlation.

www.manaraa.com
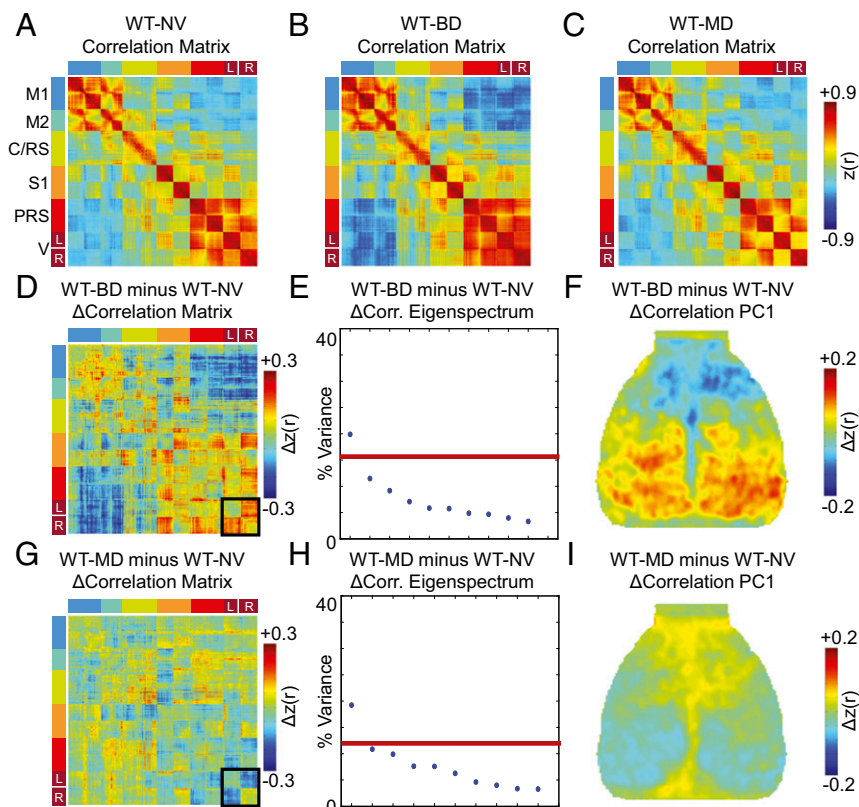
Fig. 4. Unbiased correlation analysis over the entire cortex reveals differential influence of BD and MD on intra- and internetwork correlation. (*A*–*C*) Group level correlation matrices showing correlation between every pixel pair for pixels located within RSNs for (*A*) WT-NV, (*B*) WT-BD, and (*C*) WT-MD mice. The RSN pixels have been sorted as in Fig. 2 *B* and *D*. (*D*) Correlation difference matrix calculated from WT-BD minus WT-NV demonstrates how correlation for each pixel pair differs between these two groups. The visual network is highlighted in black in *D* and *G*. Thus, the black outline in *D* demonstrates increase in correlation, in WT-BD vs. WT-NV, within the visual system. (*E*) To assess the full topography of pairwise correlation changes, we applied spatial PCA to the full, unmasked correlation difference matrix. The resulting eigenspectrum (*D*) shows that there is one statistically significant PC (red line corresponds to $P <$ 0.05, corrected; threshold computed by permutation resampling). (*F*) Topography of the significant PC, from which we term Δcorrelation PC1, indicates increased correlation between homotopic visual areas, and decreased correlation in the somatomotor system and cingulate areas, in accordance with the primary features of the difference correlation matrix (*C*). (*G*) Correlation difference matrix calculated as WT-MD minus WT-NV. (*H*) The eigenspectrum resulting from spatial PCA applied to the full, unmasked correlation difference matrix shows that there is one statistically significant PC. (*I*) Topography of the Δcorrelation PC1 indicates decreased correlation in the visual system, and increased correlation in the somatomotor system and cingulate areas.

whole-cortex Δcorrelation matrix to PCA. True differences in ISA correlation relationships that exist between groups manifest as eigenvectors accounting for variance greater than that expected by chance, as assessed through permutation resampling (see *Methods* for further details). The topography of any statistically significant PC provides a spatial summary of correlation changes between groups (this strategy for assessing correlation differences has been previously applied in ref. 20; see *Methods* for further details). This approach to statistical significance does not depend on the choice of RSNs, because every pixel is included in this PCA approach. Using this method, we found one statistically significant PC (termed a Δcorrelation PC) for the correlation differences between WT-NV vs. WT-BD (Fig. 4*E*). A map of this Δcorrelation PC1 demonstrates a pronounced increase in the posterior cross-hemispheric correlation in addition to anterior–posterior anticorrelation (Fig. 4*F*). This result is consistent with the findings from the visual-seeded correlation analysis (Fig. 3*D*) and the qualitative assessment of the RSN-sorted Δcorrelation matrices (Fig. 4*D*), which showed increased visual homotopic correlation and increased visual–anterior area anticorrelation. One statistically significant PC was also found in the WT-NV vs. WT-MD correlation difference (Fig. 4*H*). The corresponding WT-MD vs. WT-NV Δcorrelation PC1 map showed decreases in posterior correlation values and increases in anterior correlation values (Fig. 4*I*). Compared with the WT-BD vs. WT-NV Δcorrelation PC1 (Fig. 4*F*), the WT-MD vs. WT-NV Δcorrelation PC1 showed changes of opposite direction, albeit with much lower magnitude.

Visual Deprivation Does Not Alter ISA Correlation in Arc⁻/⁻ Mice. The previous experiments established an experimental model for experience-dependent ISA correlation plasticity in mice. To examine the role of synaptic plasticity in vision-mediated ISA changes, we used the same visual deprivation paradigm in Arc⁻/⁻ mice. It is important to note that Arc⁻/⁻ mice are viable, fertile, and

have normal anatomy and growth curves. Furthermore, Arc⁻/⁻ mice have normal lateral geniculate nucleus anatomy and visual cortex retinotopy (42), and cortical neuron membrane excitability is not altered (43). Additionally, Arc⁻/⁻ mice have precritical period visual-evoked potentials that are identical to those found in WT (42). Although the visual system in precritical period Arc⁻/⁻ mice appears normal, profound experience-dependent changes that occur during or after the critical period are absent or attenuated: in Arc⁻/⁻ mice, ODP plasticity was absent after monocular deprivation (42); selective responses potentiation did not occur with repeated visual presentation (42); and visual orientation learning was attenuated in adult Arc⁻/⁻ mice (44). Taken together, these results suggest that experience-dependent processes that are attenuated in Arc⁻/⁻ mice are not attributable to developmental aberrations that disrupt basic visual functionality, but the specific action of Arc on experience-driven synaptic change.

Before any correlation analysis, we examined ISA spectral content in Arc⁻/⁻ groups. We found that ISA power was equivalent between all WT and Arc⁻/⁻ groups, demonstrating equal amounts of spontaneous ISA was present in all groups (Fig. S2). Left visual-seeded correlation maps in all Arc⁻/⁻ groups exhibit the same features as those seen in WT mice: homotopic visual correlations and posterior–anterior anticorrelation (Fig. 5 *A*–*C*). However, in stark contrast to the WT mice, the correlation maps appeared nearly identical across Arc-NV, Arc-BD, and Arc-MD mice. Cluster analysis revealed no statistically significant differences in left visual-seeded correlation maps between Arc-BD and Arc-NV (Fig. 5*D*) or Arc-MD and Arc-NV (Fig. 5*E*). Furthermore, the correlation histograms for both visual–visual and visual–nonvisual connection showed no statistically significant group differences (Fig. 5 *F* and *G*). In addition, comparison of WT-BD vs. Arc-BD and WT-MD vs. Arc-MD revealed ISA correlation differences nearly identical to those seen when comparing manipulated (BD or MD) WT mice to WT-NV mice, further demonstrating the requirement for Arc in ISA correlation changes (Fig. S3).

Kraft et al.
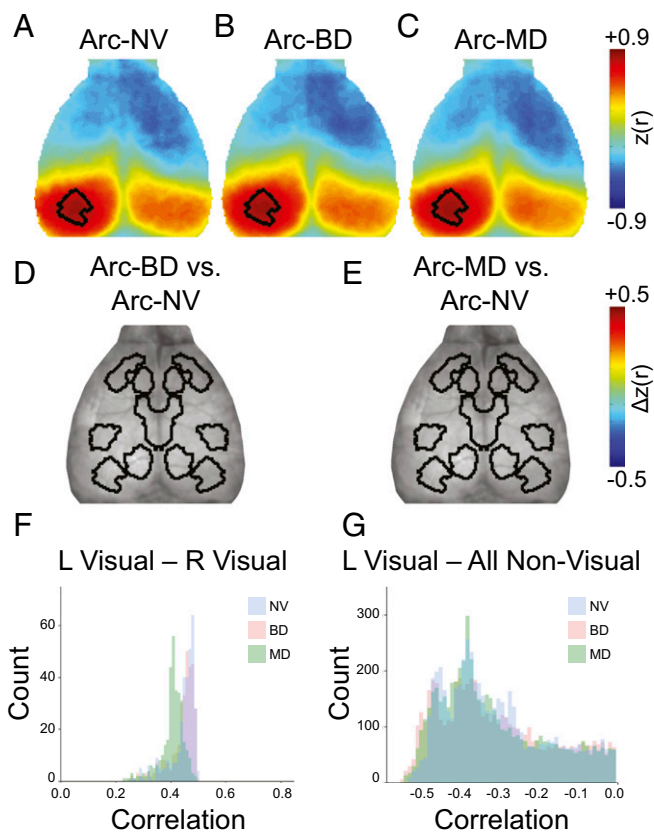
Fig. 5. Visual deprivation does not induce visual-seeded ISA correlation change in Arc$^{-/-}$ mice. (*A–C*) Group-level correlation maps seeded in the left visual RSN in (*A*) Arc-NV, (*B*) Arc-BD, and (*C*) Arc-MD mice. (*D* and *E*) Neither BD nor MD resulted in statistically significant correlation differences compared with NV in Arc$^{-/-}$ mice based on spatial clusterwise threshold-extent criteria. (*F*) Correlation histograms between all right visual RSN pixels and the left visual RSN. (*G*) Correlation histograms between all nonvisual pixels (both within and outside of RSNs in Fig. 2*B*) and the left visual RSN.

At the whole-cortex level, RSN-sorted correlation matrices were very similar between all three Arc$^{-/-}$ groups (Fig. 6 *A–C*). Examination of the Δcorrelation matrices from Arc-BD minus Arc-NV and Arc-MD minus Arc-NV comparisons demonstrated markedly attenuated ISA correlation differences compared with those seen in WT mice (Fig. 6 *D* and *F*). Furthermore, PCA revealed no statistically significant Δcorrelation PCs for Arc-BD minus Arc-NV or Arc-MD minus Arc-NV (Fig. 6 *E* and *G*). Importantly, although global signal regression (GSR) was used on our data analysis, we found that the overall topography of ISA correlation differences between groups was not altered when GSR was removed from the processing stream, suggesting that genotype-related differences in the global signal did not contribute the observed differences in FC (Fig. S4). Taken together, these results establish the role of Arc-mediated synaptic plasticity in experience-dependent ISA correlation plasticity. Moreover, these Arc-mediated changes in ISA correlation were not confined to the visual network, but manifested between distant networks as seen with BD manipulation.

Visual Deprivation Alters ISA Propagation Latency. Recent work in humans has demonstrated reproducible patterns of ISA propagation latency within and between brain regions (20, 21). Propagation latency can be quantified by calculating temporal delays between spontaneous activity measured at pixel pairs. Like ISA correlation, ISA propagation latency patterns can be modified by experience (21). To determine how early visual experience influences propa-

gation latency patterns, we examined ISA propagation latency over the whole-cortex relative to visual activity in our WT and Arc$^{-/-}$ mice (Fig. 7). The methodology for computing these propagation latency maps has been described previously (20, 21) (*Methods*). In brief, we compute the activity correlation curve between every pair of pixels in mouse cortex. The time corresponding to the peak of the latency correlation curve is the propagation delay (or latency) between the pair of signals. We can thereby calculate a latency value for every pair of pixels in the mouse cortex. As with our correlation analysis, we chose to examine latencies for each pixel relative to the average signal of all left visual RSN pixels, and used this analysis to produce a left visual-seeded latency map for each experimental group (Fig. 7 *A–F*).

Examination of the visual-seeded latency maps revealed common features between all WT and Arc$^{-/-}$ groups. Broadly, the mouse ISA latency patterns exist both between and within RSNs as has been seen in human fMRI data (20). Latency maps in both genotypes and all visual deprivation conditions were roughly symmetrical and showed common early (blue) and late (red) areas. In all groups, visual area activity was early relative to motor area activity, consistent with fMRI data from sleeping humans (20). However, quantitative group differences were apparent. To determine which changes after visual deprivation (BD and MD) were statistically significant, we applied spatial clusterwise threshold-extent criteria to the relevant within-genotype Δlatency maps (Fig. 7 *G–J*).

Compared with WT-NV, both WT-BD and WT-MD showed widespread changes in propagation latency. More specifically, BD resulted in elongated propagation time from motor to visual areas and visual to cingulate/retrosplenial areas; motor area activity occurred earlier (blue) and cingulate/retrosplenial area activity occurred later in WT-BD mice compared with WT-NV mice. Latency change occurred at the anterior edge of cingulate/retrosplenial RSN, in a region we identify as centered in the cingulate, using the same logic as in Fig. 3 (Fig. S1). Propagation latency was altered in distinct locations within the visual area (Fig. 7*G*). Similarly, MD in WT mice resulted in slowing of motor–visual–cingulate signal propagation. However, changes within the visual area resulting from MD were exclusive to the left hemisphere (contralateral to the deprived eye) and included slowed propagation to the adjacent sensory area and lateral extra visual area (Fig. 7*H*). In sum, BD and MD resulted in cross-modal ISA propagation latency changes between visual and extravisual areas separated by both short and long cortical distances.

In the Arc$^{-/-}$ groups, Δlatency maps thresholded for statistical significance revealed markedly attenuated changes attributable to visual deprivation (Fig. 7 *I* and *J*). Nonetheless, a subset of the latency changes that occurred in WT mice were also found in the absence of Arc, but Δlatency magnitude within these clusters was attenuated in the Arc$^{-/-}$ groups. Compared with Arc-NV mice, Arc-BD demonstrated propagation slowing within the visual RSN bilaterally but lacked the motor and cingulate latency increases seen in WT mice (Fig. 7*I*). Furthermore, Arc-MD mice showed the same unilateral latency changes near the visual area seen in WT-MD, but the motor and cingulate area latency changes were absent (Fig. 7*J*). Thus, experience-dependent ISA propagation plasticity was attenuated but not completely absent in Arc$^{-/-}$ mice. The cross-modal latency changes that occurred adjacent to the left visual RSN in WT mice were present in the Arc$^{-/-}$ mice, but more distant latency effects of visual deprivation were not observed.

Discussion

The effects of critical period visual experience on sensory-evoked neuronal and microcircuit responses in the visual cortex have been well-characterized; however, its impact on whole-cortex spontaneous ISA correlation and propagation patterns has not been examined. In this study, we utilized wide-field optical imaging in mice, experimentally manipulating visual experience

Kraft et al.
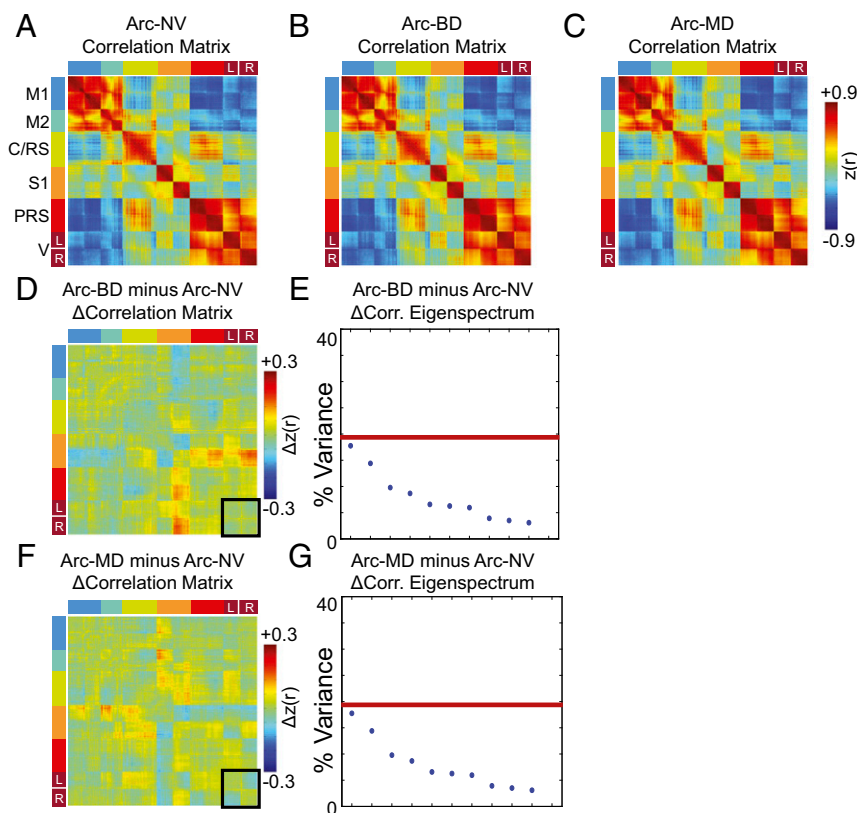
Fig. 6. Whole-cortex correlation ISA is not altered by visual deprivation in Arc$^{-/-}$ mice. (A–C) Group level correlation matrices showing correlation between every pixel pair for pixels located within RSNs for (A) Arc-NV, (B) Arc-BD, and (C) Arc-MD mice. The pixels have been ordered as in Fig. 2 B and D. (D) Correlation difference matrix calculated from Arc-BD minus Arc-NV demonstrates how correlation for each pixel pair differs between these two groups. The visual network is highlighted in black in D and F. (E) The eigenspectrum resulting from spatial PCA to the full, unmasked correlation difference matrix shows no statistically significant PCs (red line corresponds to $P < 0.05$, corrected; threshold computed by permutation resampling). (F) Correlation difference matrix calculated from Arc-BD minus Arc-NV demonstrated how correlation for each pixel pair differs between these two groups. (G) The eigenspectrum resulting from spatial PCA to the full, unmasked correlation difference matrix shows no statistically significant PCs.

during the critical period, to examine effects on network-scale ISA plasticity. We found that BD and MD induced distinct effects on intra- and internetwork spontaneous ISA correlation and propagation. Moreover, we found that these effects were attenuated in Arc$^{-/-}$ mice.

Binocular Visual Deprivation Alters Intra- and Internetwork Relationships in Spontaneous ISA Correlation. In WT mice, BD enhanced spontaneous ISA correlation across hemispheres within the visual RSNs. Work in experimental animals has shown that complete visual deprivation stalls the critical period, preventing the development of mature response features (1, 2, 4, 6–8, 12, 45). We were surprised to find that BD increased homotopic visual functional connectivity, given that decreased ISA correlation generally is a reliable biomarker of CNS disease (46, 47). Rather, these findings suggest that normal visual development results in "functional pruning" that tunes correlation in spontaneous activity between homotopic visual hemicortices to a specific range.

At the level of individual neurons, BD is known to impair the maturation of feature detection (4, 5, 7, 8). During normal development, visual cortex neurons become more selective, for both receptive fields and specific features, the differences encoded in individual visual cortex neurons may become increasingly divergent. With each visual hemicortex being largely monocular in mice, normal visual disparity between separate visual fields may result in decreased visual homotopic correlation.

In addition to altering visual intranetwork correlation, we found that BD altered internetwork correlation between visual

and extravisual networks. We observed enhanced anticorrelation between visual areas and cingulate/retrosplenial as well as contralateral motor cortex. Thus, we infer that visual experience influences the cross-modal spontaneous communication between visual and extravisual regions, and this may be a novel aspect of cross-modal plasticity.

The concept of cross-modal plasticity was initially suggested by the observation that blind or deaf individuals have heightened auditory or visual perception, respectively (48, 49). Although these findings are currently debated, it is clear that loss of a single sensory modality alters anatomical and functional relationships between distinct brain systems (30, 31, 48–51). Cross-modal plasticity has been demonstrated by physiologic and molecular assays in humans (30, 31), cats (52), rodents (50), and even *Caenorhabditis elegans* (53), which suggests it is a generalizable property of the nervous system. We suggest that enhanced internetwork correlation of ISA observed after BD (among visual, cingulate, and motor networks) may be a signature of cross-modal plasticity.

In experimental animals, visual deprivation results in enhanced axonal sprouting between the deprived visual area and surrounding auditory and somatosensory areas (52, 54–56). In addition to anatomic change, cross-modal plasticity also involves homeostatic plasticity mechanisms that drive alterations in synaptic strength. Enhanced evoked responses to auditory and tactile stimuli have been reported in mice within days of deprivation (50). Congenitally blind humans exhibit widespread changes in ISA correlation in multiple networks (30, 31), suggesting that cross-modal plasticity involves altered spontaneous activity relationships over long

Kraft et al.
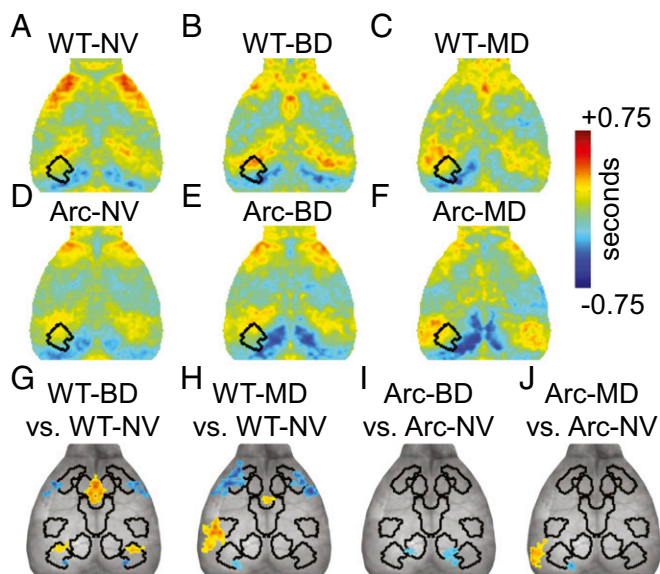
Fig. 7. BD and MD result in selective short- and long-distance propagation latency changes involving visual, motor, and cingulate/retrosplenial areas; long-distance latency changes appear to be Arc dependent. (*A–C*) Propagation latency relative to the left visual RSN in WT groups: (*A*) WT-NV, (*B*) WT-BD, and (*C*) WT-MD. (*D–F*) Propagation latency relative to the left visual RSN in Arc$^{-/-}$ groups: (*D*) WT-NV, (*E*) WT-BD, and (*F*) WT-MD. (*G*) Statistically significant differences in propagation latency between WT-BD and WT-NV mice based on spatial clusterwise threshold-extent criteria. Statistically significant differences in propagation latency between (*H*) WT-BD and WT-NV mice, (*I*) Arc-BD and Arc-NV mice, and (*J*) Arc-BD and Arc-NV mice.

distances. Caution may be appropriate in the interpretation of these human studies as they may be confounded by heterogeneous pathologic etiologies (30, 31). Moreover, Braille experience is common in blind individuals (30), and it has been argued that decades of Braille use may drive these changes (32). Our results suggest that these cross-network changes in ISA correlation can occur rapidly during the critical period (over 2 wk in this study), and do not require lifetime use of an adaptive behavior. In this regard, it may be noted that enhanced cross-modal somatosensory performance has been reported in sighted humans following only 5 d of blindfolding (57). It is interesting to speculate that these rapid changes may precede and even facilitate the development of adaptive behaviors. Future studies will be required to understand the consequences of these internetwork changes.

Monocular Visual Deprivation Induces Intranetwork Change in Spontaneous ISA Correlation Opposite to Those Seen with Binocular Deprivation. MD induces ocular dominance plasticity, which depresses the deprived eye responses and strengthens the spared eye responses (4, 6, 58, 59). Although the binocular zone is limited in mice, the deprived monocular zone undergoes visual response depression (59). This process manifests physiologically as changes in the visual response amplitude ratio between the spared and deprived eye (1, 2, 4–7, 58, 59). In this study, we find that MD induces diminished homotopic visual correlation.

The opposed effects of BD vs. MD (compared with normal vision) suggest that the correlation of spontaneous ISA between visual hemicortices matches sensory input. Indeed, MD causes more sensory discordance between each hemisphere than either BD or NV. Moreover, previous work using MD has shown that interhemispheric inhibition through callosal inputs weakens deprived eye-evoked responses (60). It has been hypothesized that interhemispheric inhibition (IHI) is an essential component of cortical brain development (61), and increased interhemispheric inhibition is thought to limit spontaneous correlation between

homotopic brain regions (46, 62, 63). Indeed, increased IHI after MD is consistent with the decreased spontaneous ISA correlation resulting from MD in our data. Hypothetically, the interhemispheric inhibition provided by transcallosal connections may also contribute to the functional pruning that tunes ISA correlation between the visual hemicortices.

Modest correlation changes between visual and extravisual areas were observed after MD. However, these changes were spatially limited and of lesser magnitude to those seen after BD. Thus, the MD-induced changes appear to be much more concentrated within the visual system. Because MD alters visual experience while BD "eliminates" visual experience, it is not surprising that extravisual changes in ISA are less affected in MD than in BD. However, it remains unclear why the extravisual changes that do occur in MD mice tend toward the direction opposite to those in BD. These differences are likely to stem from the distinction between a brain that is rewiring visual–motor circuits to adapt to altered vision (MD), as opposed to the adaptations necessary to achieve motor coordination in the absence of vision (BD).

ISA Propagation Latency Plasticity Is Distinct but Overlaps with ISA Correlation Plasticity. In addition to spatial correlation relationships, experience has been shown to alter propagation latency patterns in ISA (21). Indeed, our data demonstrate that visual experience influences ISA propagation latencies in many of the same regions showing altered correlation. In mice with NV, our visual-referenced latency maps demonstrate early visual activity and late motor activity (Fig. 7*A*), a hallmark of human activity propagation during sleep (20). Following either BD or MD, motor activity was early shifted, whereas cingulate area activity was delayed (Fig. 7 *A–D* and *H*). These effects may reflect disruption of the visual–cingulate–motor circuit following visual deprivation.

The most prominent disparity in propagation latency plasticity induced by BD vs. MD was observed near the visual RSN: in MD, these changes occurred only in the deprived hemisphere, whereas in BD these changes occurred in both hemispheres (both of which were deprived). The contrasting differences seen in correlation vs. propagation change demonstrate the distinct nature of these ISA features. Propagation latency changes induced by BD vs. MD were quite similar in areas distant from the visual cortex. In contrast, the correlation changes induced by BD vs. MD were distinct, suggesting that the experience-dependent changes in spontaneous ISA propagation latency and correlation reflect different aspects of plasticity in cross-modal communication between functional systems.

These results suggest that visual area relationships with both motor and cingulate/retrosplenial regions appear especially sensitive to visual deprivation; similar findings have been observed in early blind humans (30). Previous work has demonstrated that rodent cingulate cortex has reciprocal connections with the visual area and projects to motor areas (64, 65). In addition, visual stimulation can elicit evoked responses in the cingulate cortex (66), and direct electrical stimulation of cingulate cortex can elicit movement (67–69). Thus, converging evidence suggests that the cingulate cortex plays a role in integrating sensory information to generate behavioral outputs. Accordingly, we speculate that altered ISA relationships between visual and cingulate/retrosplenial cortex in BD mice reflects reorganization of the brain in the absence of visual input.

More broadly, our findings extend the principle, previously articulated in human studies, that the organization of spontaneous ISA is subject to experience-dependent plasticity. Several examples of this phenomenon have been described in humans: the correlation and propagation structures of the BOLD signal are known to be altered after motor learning (21, 70). Correlation changes have been reported in the context of examination preparation (29) as well as lifelong absence of vision (30, 31). The present results, obtained on the basis of fOIS imaging of

mouse cortex, demonstrate that visual experience during the mouse critical period also induces marked changes in the correlation and propagation structure of spontaneous ISA. Therefore, although the molecular basis of experience-dependent plasticity in the organization of spontaneous ISA remains unexplored in humans, the present paradigm offers an opportunity to probe the molecular bases of this reorganization in the mouse.

Arc Dependence of Spontaneous ISA Plasticity. All of the changes in correlation induced by visual manipulation (intranetwork changes in MD, and internetwork changes in BD) were absent in $Arc^{-/-}$ mice. Similarly, changes in propagation latency were largely attenuated in $Arc^{-/-}$ mice. These results suggest that Arc expression is required for experience-dependent changes in spontaneous activity correlation and propagation patterns that occur during the visual critical period.

Previous work has shown that visually evoked responses in $Arc^{-/-}$ mice are identical to WT mice before the critical period, but $Arc^{-/-}$ failed to undergo experience-dependent changes elicited by visual experience. More specifically, $Arc^{-/-}$ mice did not exhibit ocular dominance plasticity with visual deprivation or stimulus-selective response potentiation after repeated visual presentations (42). A role for Arc in experience-dependent plasticity has been demonstrated more broadly in additional settings: adult $Arc^{-/-}$ mice have attenuated visual orientation learning with repeated orientation presentation (44); $Arc^{-/-}$ mice have profound deficits in memory consolidation, and brain slices from $Arc^{-/-}$ mice show attenuated LTP and LTD (71).

Several studies have implicated Arc as a key regulator of structural, Hebbian, and homeostatic synaptic plasticity (33). More specifically, Arc has been shown to influence dendritic spine dynamics, LTP and LTD durability, and whole-neuron synaptic scaling. The best understood mechanism by which Arc influences plasticity concerns its regulation of synaptic strength via control of glutamate receptors. Arc regulates glutamate receptor levels at multiple scales, from individual synapses to the entire neuron (34–37). At the individual synapse level, Arc has been shown to target silent dendrites during activation of adjacent dendrites in the same neuron (36). Through this mechanism, Arc facilitates the selective removal of silent synapses. In addition, Arc has been shown to translocate to the nucleus and initiate whole-neuron decreases in glutamate receptor production, enabling scaling of synaptic strength throughout the entire neuron (35, 37).

Given the profound control that Arc exerts on synaptic strength, it is reasonable to hypothesize that Arc has a role in maintaining systems-level organization of the brain by modulating synaptic strength between distinct brain systems. In accordance with this view, our experiments demonstrate that $Arc^{-/-}$ mice fail to exhibit the changes in the systems-level organization of spontaneous ISA that normally occur during the visual critical period. We were surprised that visual deprivation in $Arc^{-/-}$ mice modulated the short-distance temporal ISA patterns, but not the longer-distance correlation or temporal relationships that occurred in WT mice. Thus, Arc, which is capable of selective synapse removal on the basis of activity, may be especially important in regulating both the interhemispheric connections within the visual network and the long-distance, cross-modal connections between visual and extravisual modalities. Indeed, it is well known that Arc acts locally within the visual system for vision-induced plasticity (42, 44). However, additional mechanisms that drive deprivation-induced ISA latency change within and near the visual system must exist.

Importantly, prior studies have shown that Arc gene deletion does not alter growth curves, visual system anatomy, visual cortex retinotopic maps, visual-evoked potentials, or cortical neuron membrane excitability (42–44). Thus, the experience-dependent processes that were attenuated in $Arc^{-/-}$ mice are not attributable to disrupted basic visual functionality, but to specific action of Arc on experience-driven synaptic change. Similarly, we show here that WT and $Arc^{-/-}$ mice exhibit equivalent ISA spectral content, demonstrating that spontaneous brain activity was equally abundant in both WT and $Arc^{-/-}$ mice (Fig. S2), but the reorganization of ISA spatiotemporal organization was attenuated in the absence of Arc.

To conclude, our results demonstrate that critical-period visual experience dramatically alters correlation and propagation latency patterns in spontaneous neural activity, both within and outside the visual cortex. Widespread alterations in neural activity after such a dramatic intervention are not surprising: a mouse with intact vision must interact with its environment very differently compared with a mouse without any vision (BD), or a mouse with limited vision (MD). Different experience-dependent activity patterns (normal vision vs. BD vs. MD) induce the brain to converge on distinct systems-wide patterns of neural communication, as reflected by the organization of spontaneous ISA. The process of transducing experience-dependent activity patterns into altered functional organization undoubtedly requires synaptic plasticity, and our results imply that Arc-dependent mechanisms play a role in this process. It is plausible that the local activities of Arc at the single synapse and whole-neuron level are sufficient to coordinate systems-wide reorganization on the basis of coordinated experience-dependent activity. Future studies are required to investigate these possibilities. Nonetheless, despite these mechanistic uncertainties, our results clearly establish that Arc-mediated molecular plasticity mechanisms, previously studied at a fine spatial scale, are also relevant for understanding the reorganization of neural activity at a systems level.

Limitations. All imaging performed in this study was done under ketamine/xylazine anesthesia. Although anesthesia alters spontaneous neural activity, recent work in mice has shown that cortical correlations in slow activity are quite stable across wake and ketamine/xylazine anesthesia states (72). This is in agreement with data showing stability of low-frequency correlation across states of consciousness in humans (73). Moreover, although the slow wave phenomenon was first reported in the context of anesthesia and slow wave sleep (74, 75), recent work has also shown that slow wave propagation is also present in awake rodents (76). Thus, in light of the work showing stability in low-frequency correlations and propagation across states, it is very likely that the main findings of the paper are not driven by state effects.

Methods

Mice. All procedures described below were approved by the Washington University Animal Studies Committee in compliance with Association for Assessment and Accreditation of Laboratory Animal Care guidelines. Male and female $Arc^{+/+}$ and $Arc^{-/-}$ mice (RRID:IMSR_JAX:007662) on a pure C57Bl6/J background were raised in standard cages in a dedicated mouse facility with a 12–12 light/dark cycle. Pups were weaned at P21 and immediately subjected to suturing.

Lid Suture. Mice from the same litter were randomly assigned to right monocular lid suture, binocular lid suture, or no suturing (normal vision). P21 mice were anesthetized using isoflurane until unresponsive to toe pinch. Lid margins were trimmed using fine surgical scissors and sutured shut. Normal-vision mice were subjected to equal lengths of anesthesia. After suturing, mice were kept in standard cages with 4–5 mice total in a semiclean facility with a 12–12 light/dark cycle until P35.

Imaging Animal Prep. In accord with our previously published animal preparation protocol for fOIS imaging (24), anesthesia was initiated via i.p. injection with a bolus of ketamine/xylazine (1× dose: 86.9 mg/kg ketamine, 13.4 mg/kg xylazine) and animals were allowed 15 min for anesthetic transition. After induction, the animal was placed on a heating pad maintained at 37 °C via feedback from a rectal probe (mTCII; Cell MicroControls) and its head secured in a stereotactic frame. The head was shaved and cleaned, a midline incision

www.manaraa.com

was made along the top of the head to reflect the scalp, and the skull was kept intact.

Image Acquisition. Sequential illumination was provided at four wavelengths by a ring of light-emitting diodes (LEDs) placed ~10 cm above the mouse's head. The field of view included most of the cerebral cortex (~1 cm²). Diffuse reflected light was detected by a cooled, frame-transfer EMCCD camera (iXon 897; Andor Technologies); the LED ring and the camera were time-synchronized and controlled via computer using custom-written software (MATLAB; MathWorks) at a full frame rate of 30 Hz.

Image Processing. Data from all mice were subjected to an initial quality check before spectroscopic analysis. Data runs (5 min) in which reflected light level intensity (mean value over the brain) varied as a function of time by greater than 1% for any wavelength were excluded from further analysis. This preliminary quality control yielded 10–30 min of data per mouse. For subsequent analysis, image light intensity at each wavelength was interpreted using the modified Beer–Lambert law, usually expressed as $\Phi(\mathbf{r}, t) = \Phi_0 * \exp(-\Delta\mu_a(\mathbf{r}, t) * L)$. Here, $\Phi(\mathbf{r}, t)$ is the measured light intensity, Φ_0 is the baseline light intensity, $\Delta\mu_a(\mathbf{r}, t)$ is the change in absorption coefficient due to hemodynamic changes, and L is the optical path length factor for photons in the tissue (77). Because there is no prestimulus baseline in resting-state experimentation, we normalized relative to the average light intensity at each pixel, resulting in differential measures of absorption at each wavelength at each pixel: $\Delta\mu_{a,\lambda}(\mathbf{r}, t) = -\ln(\Phi_\lambda(\mathbf{r}, t)/\langle\Phi_{0\lambda}(\mathbf{r}, t)\rangle)/L_\lambda$. Absorption coefficient data were converted to hemoglobin (Hb) concentration changes by inverting the system of equations, $\Delta\mu_{a,\lambda}(\mathbf{r}, t) = E_{\lambda,i}\Delta[Hb_i](\mathbf{r}, t)$, where E is the extinction coefficient matrix, and i runs over hemoglobin species. This inversion was performed using least-squares methods, yielding changes in oxygenated hemoglobin (HbO) and deoxygenated hemoglobin (HbR) at each pixel at each time point. Differential changes in hemoglobin concentration were filtered to retain the infraslow activity/functional connectivity band (0.009–0.08 Hz) following previous human functional connectivity algorithms (19). After filtering, each pixel's time series was downsampled from 30 to 1 Hz, and all further analysis was performed only on those pixels labeled as brain using a manually constructed brain mask. The time traces of all pixels defined as brain were averaged to create a global brain signal. This global signal was regressed from every pixel's time trace to remove global sources of variance; global signal regression was applied independently on each contiguous imaging session. Finally, data from some imaging sessions exhibited strongly oscillatory activity in the 0.04- to 0.08-Hz range, which likely reflects vascular (not neural) physiology (78). Because the spectral content of the BOLD signal is known to be ~1/f (79), we excluded runs in which 50% of the power of the filtered, regressed data were found above 0.04 Hz. This quality control step excludes data strongly contaminated by oscillatory vascular artifact.

Image Coregistration. Image sequences of each mouse (as well as the brain mask for each mouse) were affine-transformed to a common atlas space determined by the positions of the junction between the coronal suture and sagittal suture (posterior to the olfactory bulb and cerebrum along midline) and lambda, as previously reported (80). Bregma was not visible in all mice, and was calculated based on the above two anatomical landmarks. The anterior–posterior stretch was set equal to the medial–lateral stretch, and all transformed images were centered at bregma. The intersection of every brain mask was calculated and made symmetric by reflection across the midline, allowing all subsequent comparisons to be performed on shared brain areas across all mice.

ISA Correlation (Functional Connectivity) Analysis. Conventional (zero-lag) functional connectivity was computed using Pearson correlation on pairs of pixel time series. In figures depicting correlation matrices, for ease of display, we show only pixels corresponding to six RSNs inferred through PCA parcellation method of the fOIS neuroimaging data from this study (Fig. 2B) that has been used to define RSNs previously (39). Briefly, regions of interest were generated by first decomposing the whole-cortex correlation matrix of the resting-state data using PCA. Using a Bayesian information criterion (81), we identified three statistically significant components in the PCA decomposition. The three significant PCA components were then converted to regions of interest by thresholding the weights in each PC at the 95th percentile of each distribution, for positive and negative values. The spatial clusters defined by this thresholding step form the six regions of interest analyzed in this study. This approach was used on all data from all groups in this study (data from all mice averaged together to calculate the average whole-cortex correlation matrix), and ROI selection was done before any analysis. We have added this description to *Methods*. Network names were assigned to PCA topographies on the basis of colocalization with Paxinos coordinates (24). Note that for analyses involving whole-brain correlation patterns, there was no ROI dependency of results.

ISA Propagation Latency Analysis. Our method for computing propagation latency between time series has been previously published (20, 21). In brief, we determine temporal propagation latency by computing lagged cross-covariance functions:

$$C_{x_1x_2}(\tau) = \frac{1}{T}\int x_1(t+\tau) \cdot x_2(t)dt,\qquad\qquad [1]$$

where τ is the latency (in units of time). The value of τ at which $C_{x_1x_2}(\tau)$ exhibits an extremum defines the temporal latency (equivalently, delay) between signals x_1 and x_2 (82). Although cross-covariance functions can exhibit multiple extrema in the analysis of periodic signals, BOLD time series are aperiodic (79, 83) and almost always give rise to lagged cross-covariance functions with a single, well-defined extremum, typically in the range ±1 s (20). We determine the extremum abscissa and ordinate using parabolic interpolation (21).

Here, we compute delays between the time series and each pixel and the mean time series extracted from a left visual cortex area of interest. This set of temporal delays defines a left visual-seeded propagation latency map.

Statistics. To assess the topography of pairwise correlation changes across conditions, we computed the difference correlation matrices, and applied spatial principal components analysis to the difference matrix. Permutation resampling between groups was used to determine the amount of variance expected in the first eigenvalue of the PCA decomposition in the null case. Eigenvalues in the true eigenspectrum exceeding the null expectation by 2.5 SDs ($P < 0.05$; red line in Figs. 3, 5, and 6) are counted as statistically significant. Statistical significance of propagation sequence differences in spatial maps (Figs. 4–6) was assessed on a clusterwise basis using threshold-extent criteria computed by extensive permutation resampling (84).

Data and Code Availability. All presented data and analysis algorithms are available upon request.

1. Crair MC, Gillespie DC, Stryker MP (1998) The role of visual experience in the development of columns in cat visual cortex. *Science* 279:566–570.
2. Fagiolini M, Pizzorusso T, Berardi N, Domenici L, Maffei L (1994) Functional postnatal development of the rat primary visual cortex and the role of visual experience: Dark rearing and monocular deprivation. *Vision Res* 34:709–720.
3. Wang BS, Sarnaik R, Cang J (2010) Critical period plasticity matches binocular orientation preference in the visual cortex. *Neuron* 65:246–256.
4. Wiesel TN, Hubel DH (1965) Comparison of the effects of unilateral and bilateral eye closure on cortical unit responses in kittens. *J Neurophysiol* 28:1029–1040.
5. Chapman B, Stryker MP (1993) Development of orientation selectivity in ferret visual cortex and effects of deprivation. *J Neurosci* 13:5251–5262.
6. Wiesel TN, Hubel DH (1963) Single-cell responses in striate cortex of kittens deprived of vision in one eye. *J Neurophysiol* 26:1003–1017.
7. Gordon JA, Stryker MP (1996) Experience-dependent plasticity of binocular responses in the primary visual cortex of the mouse. *J Neurosci* 16:3274–3286.
8. Stryker MP, Harris WA (1986) Binocular impulse blockade prevents the formation of ocular dominance columns in cat visual cortex. *J Neurosci* 6:2117–2133.
9. Kalatsky VA, Stryker MP (2003) New paradigm for optical imaging: Temporally encoded maps of intrinsic signal. *Neuron* 38:529–545.
10. Grinvald A, Lieke E, Frostig RD, Gilbert CD, Wiesel TN (1986) Functional architecture of cortex revealed by optical imaging of intrinsic signals. *Nature* 324:361–364.
11. Blasdel GG, Salama G (1986) Voltage-sensitive dyes reveal a modular organization in monkey striate cortex. *Nature* 321:579–585.
12. Snyder A, Shapley R (1979) Deficits in the visual evoked potentials of cats as a result of visual deprivation. *Exp Brain Res* 37:73–86.

www.manaraa.com

13. Mitra A, Raichle ME (2016) How networks communicate: Propagation patterns in spontaneous brain activity. *Philos Trans R Soc Lond B Biol Sci*, 10.1098/rstb.2015.0546.
14. Raichle ME (2010) Two views of brain function. *Trends Cogn Sci* 14:180–190.
15. Raichle ME (2015) The restless brain: How intrinsic activity organizes brain function. *Philos Trans R Soc Lond B Biol Sci*, 10.1098/rstb.2014.0172.
16. Arieli A, Shoham D, Hildesheim R, Grinvald A (1995) Coherent spatiotemporal patterns of ongoing activity revealed with real-time optical imaging coupled with single-unit recording in the cat visual cortex. *J Neurophysiol* 73:2072–2093.
17. Tsodyks M, Kenet T, Grinvald A, Arieli A (1999) Linking spontaneous activity of single cortical neurons and the underlying functional architecture. *Science* 286:1943–1946.
18. Purdon PL, Weisskoff RM (1998) Effect of temporal autocorrelation due to physiological noise and stimulus paradigm on voxel-level false-positive rates in fMRI. *Hum Brain Mapp* 6:239–249.
19. Fox MD, et al. (2005) The human brain is intrinsically organized into dynamic, anticorrelated functional networks. *Proc Natl Acad Sci USA* 102:9673–9678.
20. Mitra A, Snyder AZ, Blazey T, Raichle ME (2015) Lag threads organize the brain's intrinsic activity. *Proc Natl Acad Sci USA* 112:E2235–E2244.
21. Mitra A, Snyder AZ, Hacker CD, Raichle ME (2014) Lag structure in resting-state fMRI. *J Neurophysiol* 111:2374–2391.
22. Power JD, et al. (2011) Functional network organization of the human brain. *Neuron* 72:665–678.
23. Fox MD, Corbetta M, Snyder AZ, Vincent JL, Raichle ME (2006) Spontaneous neuronal activity distinguishes human dorsal and ventral attention systems. *Proc Natl Acad Sci USA* 103:10046–10051.
24. White BR, et al. (2011) Imaging of functional connectivity in the mouse brain. *PLoS One* 6:e16322.
25. Grayson DS, et al. (2016) The rhesus monkey connectome predicts disrupted functional networks resulting from pharmacogenetic inactivation of the amygdala. *Neuron* 91:453–466.
26. Stafford JM, et al. (2014) Large-scale topology and the default mode network in the mouse connectome. *Proc Natl Acad Sci USA* 111:18745–18750.
27. Laumann TO, et al. (2015) Functional system and areal organization of a highly sampled individual human brain. *Neuron* 87:657–670.
28. Lewis CM, Baldassarre A, Committeri G, Romani GL, Corbetta M (2009) Learning sculpts the spontaneous activity of the resting human brain. *Proc Natl Acad Sci USA* 106:17558–17563.
29. Mackey AP, Miller Singley AT, Bunge SA (2013) Intensive reasoning training alters patterns of brain connectivity at rest. *J Neurosci* 33:4796–4803.
30. Burton H, Snyder AZ, Raichle ME (2014) Resting state functional connectivity in early blind humans. *Front Syst Neurosci* 8:51.
31. Wang D, et al. (2014) Altered resting-state network connectivity in congenital blind. *Hum Brain Mapp* 35:2573–2581.
32. Heine L, et al. (2015) Prevalence of increases in functional connectivity in visual, somatosensory and language areas in congenital blindness. *Front Neuroanat* 9:86.
33. Korb E, Finkbeiner S (2011) Arc in synaptic plasticity: From gene to behavior. *Trends Neurosci* 34:591–598.
34. Chowdhury S, et al. (2006) Arc/Arg3.1 interacts with the endocytic machinery to regulate AMPA receptor trafficking. *Neuron* 52:445–459.
35. Shepherd JD, et al. (2006) Arc/Arg3.1 mediates homeostatic synaptic scaling of AMPA receptors. *Neuron* 52:475–484.
36. Okuno H, et al. (2012) Inverse synaptic tagging of inactive synapses via dynamic interaction of Arc/Arg3.1 with CaMKIIβ. *Cell* 149:886–898.
37. Korb E, Wilkinson CL, Delgado RN, Lovero KL, Finkbeiner S (2013) Arc in the nucleus regulates PML-dependent GluA1 transcription and homeostatic plasticity. *Nat Neurosci* 16:874–883.
38. Smith SM, et al. (2009) Correspondence of the brain's functional architecture during activation and rest. *Proc Natl Acad Sci USA* 106:13040–13045.
39. Carbonell F, Bellec P, Shmuel A (2011) Global and system-specific resting-state fMRI fluctuations are uncorrelated: Principal component analysis reveals anti-correlated networks. *Brain Connect* 1:496–510.
40. Biswal B, Yetkin FZ, Haughton VM, Hyde JS (1995) Functional connectivity in the motor cortex of resting human brain using echo-planar MRI. *Magn Reson Med* 34:537–541.
41. Nir Y, et al. (2008) Interhemispheric correlations of slow spontaneous neuronal fluctuations revealed in human sensory cortex. *Nat Neurosci* 11:1100–1108.
42. McCurry CL, et al. (2010) Loss of Arc renders the visual cortex impervious to the effects of sensory experience or deprivation. *Nat Neurosci* 13:450–457.
43. Ren M, Cao V, Ye Y, Manji HK, Wang KH (2014) Arc regulates experience-dependent persistent firing patterns in frontal cortex. *J Neurosci* 34:6583–6595.
44. Zhao BQ, et al. (2006) Role of matrix metalloproteinases in delayed cortical responses after stroke. *Nat Med* 12:441–445.
45. McMullen CA, Andrade FH, Stahl JS (2004) Functional and genomic changes in the mouse ocular motor system in response to light deprivation from birth. *J Neurosci* 24:161–169.
46. Carter AR, et al. (2010) Resting interhemispheric functional magnetic resonance imaging connectivity predicts performance after stroke. *Ann Neurol* 67:365–375.
47. Allen G, et al. (2007) Reduced hippocampal functional connectivity in Alzheimer disease. *Arch Neurol* 64:1482–1487.
48. Bavelier D, Neville HJ (2002) Cross-modal plasticity: Where and how? *Nat Rev Neurosci* 3:443–452.
49. Pascual-Leone A, Hamilton R (2001) The metamodal organization of the brain. *Prog Brain Res* 134:427–445.
50. Petrus E, et al. (2015) Vision loss shifts the balance of feedforward and intracortical circuits in opposite directions in mouse primary auditory and visual cortices. *J Neurosci* 35:8790–8801.
51. Burton H, et al. (2002) Adaptive changes in early and late blind: A fMRI study of Braille reading. *J Neurophysiol* 87:589–607.
52. Rauschecker JP, Tian B, Korte M, Egert U (1992) Crossmodal changes in the somatosensory vibrissa/barrel system of visually deprived animals. *Proc Natl Acad Sci USA* 89:5063–5067.
53. Rabinowitch I, Bai J (2016) The foundations of cross-modal plasticity. *Commun Integr Biol* 9:e1158378.
54. Négyessy L, Gál V, Farkas T, Toldi J (2000) Cross-modal plasticity of the corticothalamic circuits in rats enucleated on the first postnatal day. *Eur J Neurosci* 12:1654–1668.
55. Toldi J, Farkas T, Völgyi B (1994) Neonatal enucleation induces cross-modal changes in the barrel cortex of rat. A behavioural and electrophysiological study. *Neurosci Lett* 167:1–4.
56. Toldi J, Rojik I, Fehér O (1994) Neonatal monocular enucleation-induced cross-modal effects observed in the cortex of adult rat. *Neuroscience* 62:105–114.
57. Merabet LB, et al. (2008) Rapid and reversible recruitment of early visual cortex for touch. *PLoS One* 3:e3046.
58. Hensch TK (2005) Critical period plasticity in local cortical circuits. *Nat Rev Neurosci* 6:877–888.
59. Ranson A, Sengpiel F, Fox K (2013) The role of GluA1 in ocular dominance plasticity in the mouse visual cortex. *J Neurosci* 33:15220–15225.
60. Restani L, et al. (2009) Functional masking of deprived eye responses by callosal input during ocular dominance plasticity. *Neuron* 64:707–718.
61. Homae F (2014) A brain of two halves: Insights into interhemispheric organization provided by near-infrared spectroscopy. *Neuroimage* 85:354–362.
62. Stagg CJ, et al. (2014) Local GABA concentration is related to network-level resting functional connectivity. *eLife* 3:e01465.
63. Antonenko D, et al. (2017) tDCS-induced modulation of GABA levels and resting-state functional connectivity in older adults. *J Neurosci* 37:4065–4073.
64. Vogt BA, Miller MW (1983) Cortical connections between rat cingulate cortex and visual, motor, and postsubicular cortices. *J Comp Neurol* 216:192–210.
65. Zhang S, et al. (2016) Organization of long-range inputs and outputs of frontal cortex for top-down control. *Nat Neurosci* 19:1733–1742.
66. Cuénod M, Casey KL, MacLean PD (1965) Unit analysis of visual input to posterior limbic cortex. I. Photic stimulation. *J Neurophysiol* 28:1101–1107.
67. Woolsey CN, Erickson TC, Gilson WE (1979) Localization in somatic sensory and motor areas of human cerebral cortex as determined by direct recording of evoked potentials and electrical stimulation. *J Neurosurg* 51:476–506.
68. Lende RA, Woolsey CN (1956) Sensory and motor localization in cerebral cortex of porcupine (Erethizon dorsatum). *J Neurophysiol* 19:544–563.
69. Kaada BR (1951) Somato-motor, autonomic and electrocorticographic responses to electrical stimulation of rhinencephalic and other structures in primates, cat, and dog; a study of responses from the limbic, subcallosal, orbito-insular, piriform and temporal cortex, hippocampus-fornix and amygdala. *Acta Physiol Scand Suppl* 24:1–262.
70. Albert NB, Robertson EM, Miall RC (2009) The resting human brain and motor learning. *Curr Biol* 19:1023–1027.
71. Plath N, et al. (2006) Arc/Arg3.1 is essential for the consolidation of synaptic plasticity and memories. *Neuron* 52:437–444.
72. Silasi G, Xiao D, Vanni MP, Chen AC, Murphy TH (2016) Intact skull chronic windows for mesoscopic wide-field imaging in awake mice. *J Neurosci Methods* 267:141–149.
73. Picchioni D, Duyn JH, Horovitz SG (2013) Sleep and the functional connectome. *Neuroimage* 80:387–396.
74. Amzica F, Steriade M (1995) Short- and long-range neuronal synchronization of the slow (< 1 Hz) cortical oscillation. *J Neurophysiol* 73:20–38.
75. Steriade M, Nuñez A, Amzica F (1993) A novel slow (< 1 Hz) oscillation of neocortical neurons in vivo: Depolarizing and hyperpolarizing components. *J Neurosci* 13:3252–3265.
76. Petersen CC, Hahn TT, Mehta M, Grinvald A, Sakmann B (2003) Interaction of sensory responses with spontaneous depolarization in layer 2/3 barrel cortex. *Proc Natl Acad Sci USA* 100:13638–13643.
77. Arridge SR, Cope M, Delpy DT (1992) The theoretical basis for the determination of optical pathlengths in tissue: Temporal and frequency analysis. *Phys Med Biol* 37:1531–1560.
78. Bumstead JR, Bauer AQ, Wright PW, Culver JP (2017) Cerebral functional connectivity and Mayer waves in mice: Phenomena and separability. *J Cereb Blood Flow Metab* 37:471–484.
79. He BJ, Zempel JM, Snyder AZ, Raichle ME (2010) The temporal structures and functional significance of scale-free brain activity. *Neuron* 66:353–369.
80. Bauer AQ, et al. (2014) Optical imaging of disrupted functional connectivity following ischemic stroke in mice. *Neuroimage* 99:388–401.
81. Minka T (2000) Automatic choice of dimensionality for PCA (MIT Media Laboratory, Vision and Modeling Group, Cambridge, MA) Technical Report 514.
82. König P (1994) A method for the quantification of synchrony and oscillatory properties of neuronal activity. *J Neurosci Methods* 54:31–37.
83. Maxim V, et al. (2005) Fractional Gaussian noise, functional MRI and Alzheimer's disease. *Neuroimage* 25:141–158.
84. Hayasaka S, Nichols TE (2003) Validating cluster size inference: Random field and permutation methods. *Neuroimage* 20:2343–2356.

Kraft et al.

www.manaraa.com